PL-TR-97-2065

# SHEAR WAVE GENERATION FROM CONTAINED EXPLOSIONS

Thomas J. Ahrens
Cangli Liu

California Institute of Technology
Seismological Laboratory 252-21
1200 E. California Blvd
Pasadena, CA 91125

18 July 1996

Scientific Report No. 1



approved for public release; distribution unlimited



PHILLIPS LABORATORY
Directorate of Geophysics
AIR FORCE MATERIEL COMMAND
HANSCOM AFB, MA 01731-3010

SPONSORED BY
Air Force Technical Applications Center
Directorate of Nuclear Treaty Monitoring
Project Authorization T/5101

MONITORED BY
Phillips Laboratory
CONTRACT No. F19628-95-C-0115

The views and conclusions contained in this document are those of the authors and should not be interpreted as representing the official policies, either express or implied, of the Air Force or U.S. Government.

This technical report has been reviewed and is approved for publication.

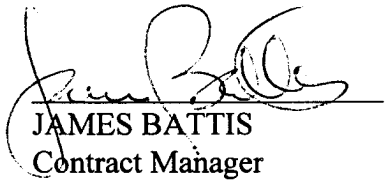

JAMES BATTIS
Contract Manager
Space Effects Division

DAVID A. HARDY
Director
Space Effects Division

This report has been reviewed by the ESD Public Affairs Office (PA) and is releasable to the National Technical Information Service (NTIS).

Qualified requestors may obtain copies from the Defense Technical Information Center. All others should apply to the National Technical Information Service.

If your address has changed, or you wish to be removed from the mailing list, or if the addressee is no longer employed by your organization, please notify PL/IM, 29 Randolph Road, Hanscom AFB, MA 01731-3010. This will assist us in maintaining a current mailing list.

Do not return copies of this report unless contractual obligations or notices on a specific document requires that it be returned.

# REPORT DOCUMENTATION PAGE

Form Approved
OMB No. 0704-0188



| 1. AGENCY USE ONLY (Leave blank) | 2. REPORT DATE | 3. REPORT TYPE AND DATES COVERED |
|---|---|---|
| | 18 July 1996 | Scientific No. 1 |

**4. TITLE AND SUBTITLE**
Shear Wave Generation from Contained Explosions

**5. FUNDING NUMBERS**
C-F19628-95-C-0115
PE 35999F
PR 5101
TA GM
WU AH

**6. AUTHOR(S)**
Thomas J. Ahrens and Cangli Liu

**7. PERFORMING ORGANIZATION NAME(S) AND ADDRESS(ES)**
California Institute of Technology
Seismological Laboratory 252-21
1200 E. California Blvd.
Pasadena CA 91125

**8. PERFORMING ORGANIZATION REPORT NUMBER**

**9. SPONSORING / MONITORING AGENCY NAME(S) AND ADDRESS(ES)**
Phillips Laboratory
29 Randolph Road
Hanscom AFB, MA 01731-3010
Contract Manager: James Battis/GPE

**10. SPONSORING / MONITORING AGENCY REPORT NUMBER**
PL-TR-97-2065

**11. SUPPLEMENTARY NOTES**

**12a. DISTRIBUTION / AVAILABILITY STATEMENT**
Approved for public release; distribution is unlimited

**12b. DISTRIBUTION CODE**

**13. ABSTRACT** *(Maximum 200 words)*

The usefulness of the amplitude ratio of seismic phases such as Lg/P, as well as the ratio of magnitudes (e.g. Mb/Ms) to discriminate explosions from earthquakes depends, in part, on the efficiency of shear wave production from seismic sources. We are studying shear wave generation at the source, initially from explosions within limestone blocks. Initially the samples are subjected to hydrostatic stress. However, we will be able to also simulate tectonic strain energy release in future experiments. Using a 1.6 m long, 0.8 m diameter sample subjected to an ambient pressure of up to 1 MPa, with a centrally placed explosive source, we propose to study the amplitude of shear wave generation of stress-wave induced radial cracking in symmetric and asymmetric cavities. In unstressed rock, this shear wave production is expected to be controlled in part by the natural anisotropy of the rock (e.g. bedding). We expect to measure the S/P ratio from tamped explosions using (0.2 to 2 gram charges). Later tests will be conducted in partially decoupled asymmetric cavities, and the resultant shear wave radiation pattern will be compared to previous detailed finite element calculations of P and S wave radiation versus frequency and angle for elliptical cavities of aspect ratios in the range of 1:3 to 1:10 conducted by Glenn et al. [1985]. In order to measure the P and S waves generated from explosions, we developed a measurement method that is given in detail in this report. The initial test results for the tamped and decoupled explosions in cylindrical cavities in limestone show that the amplitude of SV/P for the decoupled experiment in limestone is ~0.7, whereas it varies over a range of ~1 to 3 for overdriven cavities, depending on angle from the cylindrical axis. Moreover, tensional cracks are generated in these cavities which resemble those inferred to have occurred in a similar geometry in the Sterling experiment.

| 14. SUBJECT TERMS | 15. NUMBER OF PAGES |
|---|---|
| confined explosions, rocks, shear wave generation, discrimination | 38 |
| | 16. PRICE CODE |

| 17. SECURITY CLASSIFICATION OF REPORT | 18. SECURITY CLASSIFICATION OF THIS PAGE | 19. SECURITY CLASSIFICATION OF ABSTRACT | 20. LIMITATION OF ABSTRACT |
|---|---|---|---|
| unclassified | unclassified | unclassified | SAR |

CONTENTS

1. Objectives ..... 1

2. Research Accomplished ..... 1

2.1 Introduction ..... 1
2.2 Measuremental Method ..... 3
2.3 Sensors ..... 4
2.4 Data Reduction Method ..... 4

2.4.1 The P-Wave Reflection at Free Surfaces ..... 4
2.4.2 The SV-Wave Reflection at a Free Surface ..... 8
2.4.3 Strains Due to Incident P-Waves ..... 9
2.4.4 Strains Induced by Incident SV-Waves ..... 11
2.4.5 The Amplitude of Incident P- and SV-Waves ..... 11
2.4.6 The Characteristics of the Strains Given by Gauges ..... 12

3. Experiments and Results ..... 14

3.1 Experimental Details ..... 14
3.2 Experimental Results ..... 14

4. Conclusions ..... 24

References

## ILLUSTRATIONS

Page


1. (A) Layout of rock sample, strain gauges and explosive charge
   (B) Sketch of polarization directions of strain gauges.....5

2. Block diagram of shear wave generation experiments.....6

3. $H_1$ and $H_2$ versus P-3 wave incident angle ($\theta$) .....13

4. $G_1$ and $G_2$ versus the SV-wave incident angle ($\theta$).....13

5. Mechanical configuration of test chamber to study shear wave ... generation in rocks.....15

6. (a) The wave profiles from gauges 1-4.....17
6. (b) The wave profiles from gauges 5 and 6.....18

7. (a) Wave profiles from gauges 1-4 (the tamped experiment)..19
7. (b) The wave profiles from gauges 5-8.....20

8. Ratio of P- to SV-wave particle velocity, P/SV, versus explosive energy.....21

9. Profile of fracture surface from tamped experiment .....22


## TABLES

Page


1. Parameters used in the experiments.....16
2. The results for the decoupled experiment .....16
3. The results for the tamped experiment.....16

ACKNOWLEDGMENTS

The following Caltech technical and administrative personnel assisted in the construction of the apparatus, conduct of initial experiments, and preparation of this report: Victor Nenow, Michael Long, Jose Nunez-Anzueto, Alberto Devora, Epaprodito Gelle, Geoffrey Batten, and Susan Yamada.

The research reported was conducted solely under this contract. This project is sponsored by: the Air Force Technical Applications Center.

# 1 OBJECTIVES

We are conducting small-scale explosive experiments to test discrimination theories of shear wave generation from explosions in symmetric and asymmetric cavities in rocks. Small PETN charges are detonated in symmetric and asymmetric cavities, within meter-sized samples of limestone, shale, and other rock types. We constructed an apparatus (Figures 1, 2 and 5) to measure shear wave generation both from the asymmetric stress imposed on the explosion cavity walls by detonation, as well as from the cracking of the rock. We also expect to develop a theoretical model of these effects. We expect to apply Brune's (U. Nevada) and L. Glenn's (LLNL) model of the stresses from such cavities to test discrimination algorithms.

We have developed sealing methods for conducting the test under $\sim$ 1 MPa of water pressure, as shown in Fig.5. Initially rock samples of Bedford limestone were employed in the initial tests that are discussed below.

# 2 RESEARCH ACCOMPLISHED

## 2.1 Introduction

In the past 30 years, extensive research has been conducted on the discrimination of underground explosions from earthquakes. As a result, Murphy (1996) recently concluded that the seismology of earthquakes and underground explosions is at a state that it is possible to identify tamped explosions with the yield over 1 kiloton ( $m_b \geq 4$) on a world-wide basis. These explosions can be distinguished from earthquakes by the global seismic stations using the initial P-wave motion and the $M_s$ to $m_b$ ratio. In fact, the discrimination of the tamped explosions from earthquakes depends mainly on the collection of the seismic data from previous underground nuclear explosions. However, many basic problems related to tamped explosions still remain unsolved ( Masse, 1981; Murphy, 1996 ), e.g., the generation of long period Rayleigh waves ($\geq$ 5 seconds), SH-waves and Love-waves etc. But now, the most difficult problem is to distinguish earthquakes from decoupled explosions with complex geometries.

The characteristics for decoupled explosions (Murphy, 1996) are: (1) $m_b$ is too low to use the global monitoring system ( in general, $m_b \leq 3$); (2) the amplitude of surface waves generated in the explosions is much less than it is from the tamped explosions(it is hard to distinguish it from white noise); (3) the excitation of direct SV-waves and possible SH-waves makes the problem more difficult. Although there are many published papers related to the decoupled explosions (Glenn et al., 1985, 1993, 1994, 1996; Murphy et al. 1996; Murphy, 1996; Sykes, 1996; Langston, 1983 etc.), it still is unclear what really controls the generations of S-waves in decoupled explosions (Murphy, 1996). Therefore, the mechanism of S-wave generation from explosions, especially from decoupled explosions is the fundamental question for discrimination.

The suggested possible sources for S-waves from explosions include: (1) the dynamic radial fracture of the rocks near explosions; (2) the asymmetric plastic deformation near the explosion due to the asymmetric geometry and anisotropy of the rocks; (3) tectonic release of shear energy triggered by shock waves from the explosions; (4) the conversion of P-waves to S-waves at the free surface of the Earth. These mechanisms must be studied separately using different methods.

The objective of this work is to investigate shear-wave generation from dynamic fracture and the conversion of shock waves to P- and S-waves on the inner surfaces of the cavities by examining the relationship between the geometry and the amplitude distribution of the S-waves generated from confined explosions in rocks in the laboratory. For symmetric or asymmetric explosions, if the shock wave pressure is not too high, the rocks near explosions will fail via brittle fracture mechanisms. Radial fractures may be initiated from the inner surface of the cavity because the tangential(hoop) stresses always achieve the maximum on the surface. This radial fracture generally is further driven by the high-pressure explosive products (Coursen, 1985). In asymmetric explosions, the reflection of the shock waves from the inner cavity surface will also produce S-waves. The amplitude of the S-waves depends on the incident angle and generally increases with the incident angle for angles below the critical reflection angle.

In order to investigate the details of the S-wave generation from tamped and decoupled explosions in rocks, we need first to develop a measurement method that can be used to monitor both P- and S-waves generated in explosions. For small-scale laboratory experiments, the wave profiles have relatively higher frequencies than the usual seismic waves. Therefore, the conventional seismic recording system can not be used to measure those wave profiles. One candidate method developed for super-high strain rate experiments (Kim and Clifton, 1977) is difficult to employ for the present experiments because it requires special treatment of samples. Magnetic velocity gauges have been used to study shock wave decays in rocks, but this method requires embedding the gauges in the rock. This adds some artificial interfaces which will make the S-wave data more complicated. Based on the analysis of the interaction between P- and S-waves and free surfaces, we have developed a method to measure P- and S-wave profiles on the free surfaces of rocks. The main idea of the method is to use the different characteristics of the interactions between P- and S-waves and the free surface. The method and the experimental data from this method are presented below.

## 2.2 Measurement Method

When P- and S-waves arrive at the free surface, the interactions between the P- and S-waves and the free surface are very different. The characteristics of these interactions provide the opportunity to measure the incident P- and S-wave amplitudes from the strain measurements on the free surfaces of rocks. The method developed is to use two strain gauges to measure the strains along two perpendicular directions at one point on the free surface of the rocks. The incident amplitude of P- and S-waves can be obtained from these strain measurements.

The basic assumptions made for the method are:

1. The waves in the rocks can be approximately treated as locally plane waves.

2. The deformation of the rocks near the free surface is elastic.

## 2.3 Sensors

A group of strain gauges are employed to monitor the wave profiles at different locations along two directions on the free-surface of rock samples. The directions of the gauges are shown in Figure 1. The block diagram of the recording system is shown in Figure 2. The gauges and amplifiers are powered by batteries in order to achieve a high signal/noise ratio. A mercury relay is used to calibrate the system. The relation between strains, $\varepsilon$, and voltages change, $\Delta V$, is

$$\varepsilon = \frac{\Delta V}{fgV_0}, \tag{1}$$

where $V_0$ is the initial voltage supplied on the gauges. $f$ and $g$ are the gauge factor and gain of the amplifiers, respectively.

## 2.4 Data Reduction Method

Strain gauges give the elongation along the gauge directions. When they are attached on a free surface, they measure the elongation of the free surface after wave reflections. The strains recorded by the gauges include the contributions from incident P- and S-waves and the reflected P- and S-waves. In order to get the relation between the strains given by the gauges and the incident P- and S-wave amplitudes, we first conducted an analysis of the interactions between the incident P- and S-waves and the free surfaces.

### 2.4.1 The P-wave Reflection at Free Surfaces

The displacement reflection coefficients for incident P-waves at free surfaces (Aki and Richards, 1980) are

$$PP = \frac{B - A}{B + A}, \tag{2}$$

$$PS = \frac{2\frac{\beta}{\alpha}\sin(2\theta)\cos(2j)}{A + B}, \tag{3}$$

where $PP$ and $PS$ are the reflection coefficients for P- and SV-wave displacements due to the incident P-waves, respectively. $\alpha$ and $\beta$

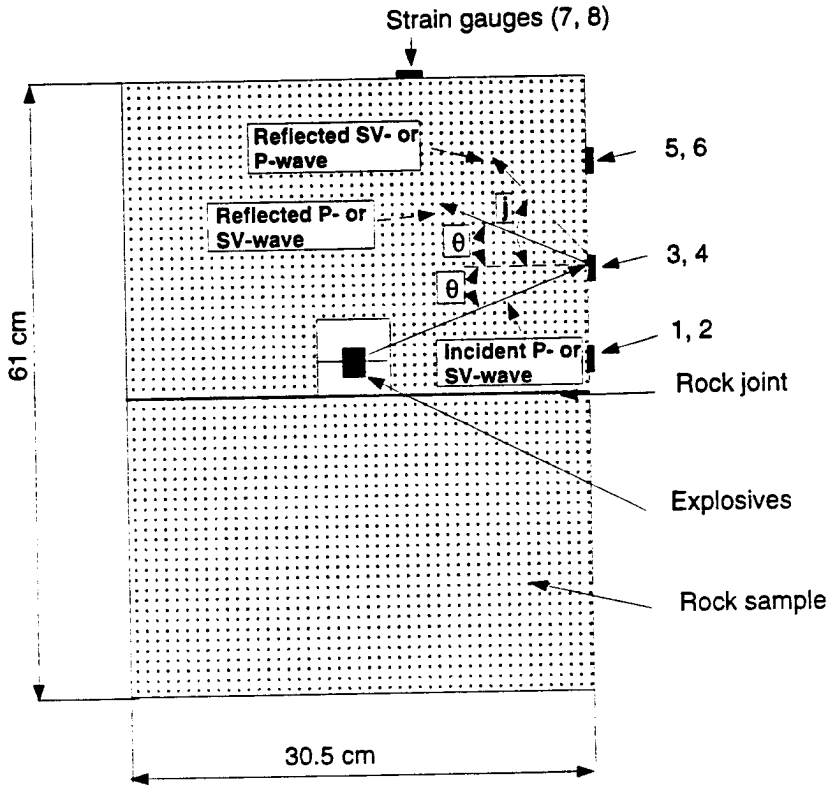


Figure 1 (A) Layout of rock sample, strain gauges and explosive charge

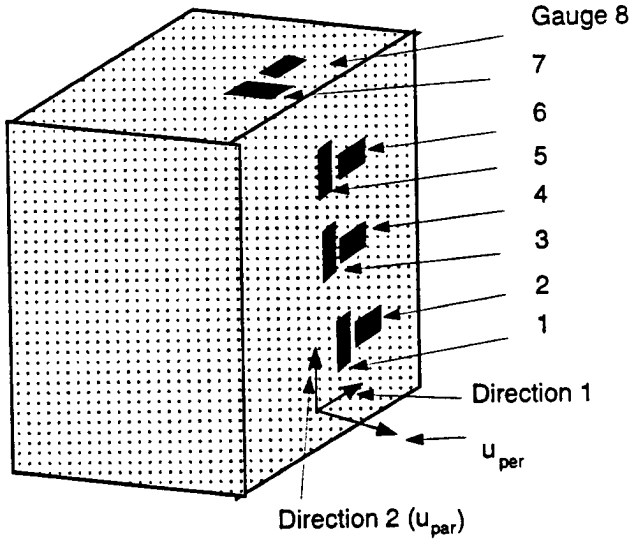


Figure 1 (B) Sketch of polarization directions of strain gauges

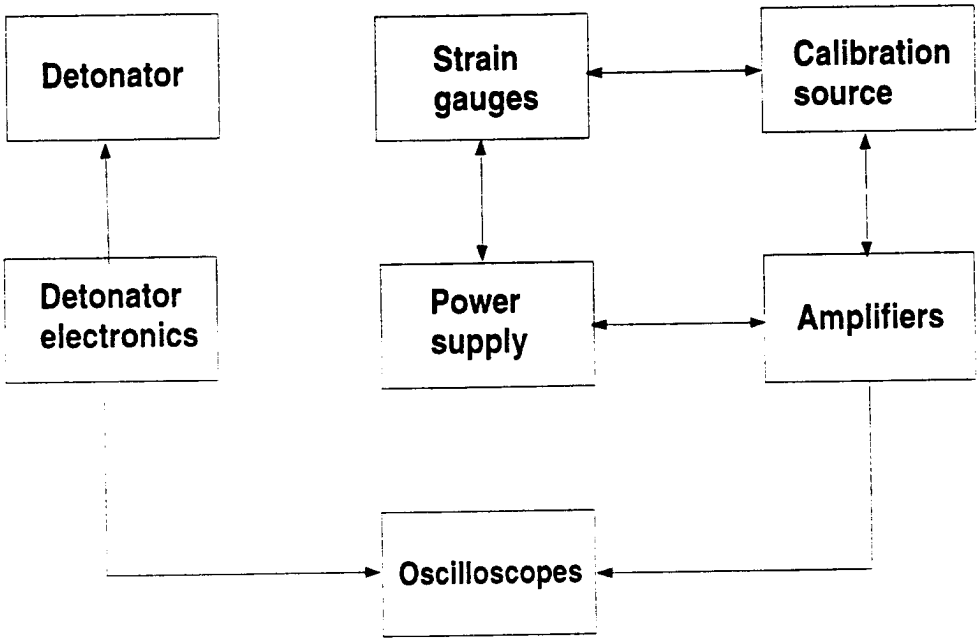


Figure 2 Recording system of the experiments

are P- and S-wave velocities, respectively. $A$ and $B$ are

$$A = \cos^2(2j), \tag{4}$$

$$B = (\frac{\beta}{\alpha})^2 \sin(2j) \sin(2\theta), \tag{5}$$

where $\theta$ and $j$ are the P-wave incident angle and S-wave reflection angle, respectively. The $\theta$ and $j$ are shown in Figure 1.

$$\sin j = \frac{\beta}{\alpha} \sin\theta, \tag{6}$$

$$\cos j = (1 - (\frac{\beta}{\alpha})^2 \sin^2 j)^{\frac{1}{2}}. \tag{7}$$

The resultant displacements of the particles on the free surfaces after the reflection are

$$u^p_{par} = u^I_p[(1 + PP)\sin\theta + PS\cos j] = H_{par} u^I_p, \tag{8}$$

$$u^p_{per} = u^I_p[(1 - PP)\cos\theta + PS\sin j] = H_{per} u^I_p, \tag{9}$$

where $u^I_p$ is the particle displacement of the incident P-wave, $u^p_{par}$ and $u^p_{per}$ indicate the resultant particle displacements along direction 2 and the direction that is perpendicular to the free surface after reflection as shown in Figure 1, respectively. The $H_{par}$ and $H_{per}$ are

$$H_{par} = (1 + PP)\sin\theta + PS\cos j, \tag{10}$$

$$H_{per} = (1 - PP)\cos\theta + PS\sin j. \tag{11}$$

Substituting all the definitions into the equations, Eqs.(10) and (11) can be rewritten as

$$H_{par} = \frac{2\cos\theta \sin(2j)}{A + B}, \tag{12}$$

$$H_{per} = \frac{2\cos\theta \cos(2j)}{A + B}. \tag{13}$$

### 2.4.2 The SV-wave Reflection at Free Surfaces

For incident SV-waves, the displacement reflection coefficients for P- and SV-waves (Aki and Richards, 1980) are

$$SP = \frac{\frac{\beta}{\alpha}\sin(4\theta)}{A_s + B_s}, \tag{14}$$

$$SS = \frac{A_s - B_s}{A_s + B_s}, \tag{15}$$

where $SS$ and $SP$ are the reflection coefficients of SV- and P-wave displacements due to the incident SV-waves.

$$A_s = \cos^2(2\theta), \tag{16}$$

$$B_s = (\frac{\beta}{\alpha})^2 \sin(2\theta)\sin(2j), \tag{17}$$

where $\theta$ and $j$ are the SV-wave incident angle and P-wave reflected angle, respectively, and

$$\cos j = (1 - (\frac{\alpha}{\beta})^2 \sin^2\theta)^{\frac{1}{2}}. \tag{18}$$

The resultant displacements of the particles on the free surfaces after the reflection are

$$u_{par}^{sv} = u_{sv}^I[(1 + SS)\cos\theta + SP\sin j] = G_{par}u_{sv}^I, \tag{19}$$

$$u_{per}^{sv} = u_{sv}^I[(SS - 1)\sin\theta - SP\cos j] = G_{per}u_{sv}^I, \tag{20}$$

where $u_{par}^{sv}$ and $u_{per}^{sv}$ are the resultant particle displacements on the free surface after reflection along direction 2 as shown in Figure 2 and the direction that is perpendicular to the free surface, respectively. $u_{sv}^I$ is the particle displacement of the incident SV-wave. The $G_{per}$ and $G_{par}$ are

$$G_{par} = (1 + SS)\cos\theta + SP\sin j, \tag{21}$$

$$G_{per} = (SS - 1)\sin\theta - SP\cos j. \tag{22}$$

Substituting all the definitions into the equations, they are rewritten as

$$G_{par} = \frac{2\cos(2\theta)\cos\theta}{A_s + B_s}, \tag{23}$$

$$G_{per} = -2\frac{\frac{\beta}{\alpha}\cos j\sin(2\theta)}{A_s + B_s}. \tag{24}$$

### 2.4.3 Strains Due to Incident P-waves

1. Strains given by the gauges along direction 1

   Because $u^p_{per}$ is perpendicular to the free surface and along the symmetrical axis direction of the waves, the strain due to $u^p_{per}$ along direction 1 is simply expressed as

   $$\varepsilon_1^{per} = \frac{H_{per}}{r_0} u_p^I, \tag{25}$$

   where $\varepsilon_1^{per}$ is the strain along direction 1 induced by $u^p_{per}$, and $r_0$ is the distance from the center of the cavity to the free surface at $\theta = 0$.

   Because $u^p_{par}$ does not result in any strains in the gauges along direction 1 at any time, the total strain induced by the incident P-waves is

   $$\varepsilon_1^p = H_1 u_p^I, \tag{26}$$

   where $H_1 = \frac{H_{per}}{r_0}$.

2. Strains given by the gauges along direction 2

   Because $u^p_{per}$ and $u^p_{par}$ all have contributions to the strain given by the gauges along direction 2, we need to consider the resultant displacements.

   The length of the gauge after the reflection, $\Delta s$, is

   $$\Delta s = (r_n^2 + (\frac{\partial r_n}{\partial \theta})^2)^{\frac{1}{2}} \delta\theta, \tag{27}$$

   where

   $$\delta\theta = \frac{l_s}{r_n}, \tag{28}$$

   and $l_s$ is the initial length of strain gauges. $r_n$ is the distance from the center of the cavity to the position of the gauge after reflections

   $$r_n = r + u\cos(\eta - \theta), \tag{29}$$

   where $r$ is the distance from the center of the cavity to the gauge before P-wave reflection, $u$ is the resultant displacement

of the point at $\theta$ on the free surface and $\eta$ is the angle between $u$ and $u^p_{per}$, they are

$$u = u^I_p \frac{2\cos(\theta)}{A+B}, \tag{30}$$

$$\eta = 2j. \tag{31}$$

To a first-order approximation, $\Delta s$, is

$$\Delta \approx ((\frac{r}{\cos\theta})^2 + 2ru^I_p(W(\theta) + \tan(\theta)\frac{dW}{d\theta})^{\frac{1}{2}}\frac{l_s\cos\theta}{r}, \tag{32}$$

where

$$W = \frac{2\cos(\theta)\cos(\eta-\theta)}{A+B}. \tag{33}$$

If $x \ll 1$, we have

$$(1+x)^{\frac{1}{2}} \simeq 1 + \frac{x}{2}. \tag{34}$$

Because $\frac{u^I_p}{r} \ll 1$, after using the approximation above, $\Delta s$ is

$$\Delta s \approx (r(1+\frac{\tan^2\theta}{2})+u^I_p(W(\theta)(1-\frac{\tan^2\theta}{2})+\tan\theta\frac{dW}{d\theta}))\delta\theta. \tag{35}$$

Then the strain is

$$\varepsilon^p_2 = \frac{\Delta s - l_s}{l_s}, \tag{36}$$

and therefore

$$\varepsilon^p_2 = H_2 u^I_p, \tag{37}$$

where

$$H_2 = \frac{(\cos\theta(W(1-\frac{\tan^2\theta}{2})+\tan\theta\frac{dW}{d\theta})}{(1+\frac{\tan^2\theta}{2})}, \tag{38}$$

and $r_0 = r\cos\theta$.

### 2.4.4 Strains Induced by Incident SV-waves

Using the same method, all the strains induced by incident SV-waves can be obtained. The final expressions are listed as following:

1. The strains given by the gauges along direction 1 are

$$\varepsilon_1^{sv} = G_1 u_{sv}^I, \tag{39}$$

where

$$G_1 = \frac{G_{per}}{r_0}. \tag{40}$$

2. The strains given by the gauges along direction 2 can be found using the same method as for the incident P-wave. The resultant strains induced by the incident SV-waves along direction 2 are

$$\varepsilon_2^{sv} = G_2 u_{sv}^I, \tag{41}$$

where

$$G_2 = \frac{(\cos\theta(W_s(1 - \frac{\tan^2\theta}{2}) + \tan\theta\frac{dW_s}{d\theta})}{(1 + \frac{\tan^2\theta}{2})}, \tag{42}$$

$$W_s = \frac{2\cos(\eta - \theta)\cos\theta}{A_s + B_s}(\cos^2(2\theta) + 4(\frac{\beta}{\alpha})^2\cos^2 j\sin^2\theta)^{\frac{1}{2}}, \tag{43}$$

$$\tan\eta = -\frac{\alpha\cos\theta}{\beta\cos j\tan(2\theta)}. \tag{44}$$

### 2.4.5 The Amplitude of Incident P- and SV-waves

From the expressions given above, the displacements of incident P- and SV-waves can be obtained through the strains given by the gauges along the two directions.

1. The displacement of the incident P-waves is

$$u_p^I = \frac{\varepsilon_1^p}{H_1} = \frac{\varepsilon_2^p}{H_2}. \tag{45}$$

2. The displacement of the incident SV-waves is

$$u_{sv}^I = \frac{\varepsilon_{sv}^1}{G_1} = \frac{\varepsilon_{sv}^2}{G_2}. \tag{46}$$

### 2.4.6 The Characteristics of the Strains Given by Gauges in Bedford Limestone

1. P-waves

   (a) The non-dimensional constant, $H_1$ in Eq.(45) is not sensitive to the variation in $\theta$, e.g., the value of $H_1$ is about 2.0 for Bedford limestone. The non-dimensional constant, $H_2$ in Eq.(45) changes rapidly with $\theta$, it varies from -0.8 to 2 for Bedford limestone as shown in Figure 3.

   (b) From Figure 3, the strains induced by P-waves along direction 1 are always positive, but the strains along direction 2 are positive when $\theta$ is less than $47^o$ and negative when $\theta$ is larger than $47^o$ ( for Bedford limestone). This polarity change is controlled by the ratio of the projection of P-wave displacement along direction 1 to that along the direction that is perpendicular to the free surface.

2. SV-waves

   (a) The relation between $G_1$ ($G_2$) and the SV-wave incident angle for Bedford limestone is given in Figure 4. From the calculated results, the gauges along direction 1 are not sensitive to incident SV-wave; however, the gauges along direction 2 are very sensitive to incident SV-wave.

   (b) The measurement of SV-waves are limited by the Rayleigh surface wave generation. For Bedford limestone, the Rayleigh wave is generated when $\theta$ is larger than about $35^o$ ( determined from Snell's law).

   (c) The polarities of the strains along direction 2 are negative, and the polarities of the strains along direction 1 are determined by the direction of the particle motion ( the calculation is made assuming that the motion direction is toward the increasing direction of the SV-wave incident angle).

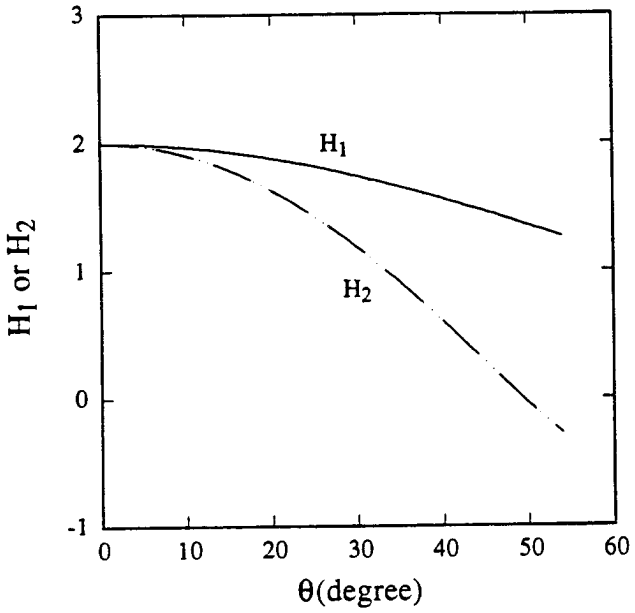


Figure 3 $H_1$ and $H_2$ versus P-wave incident angle ($\theta$) in Bedford limestone

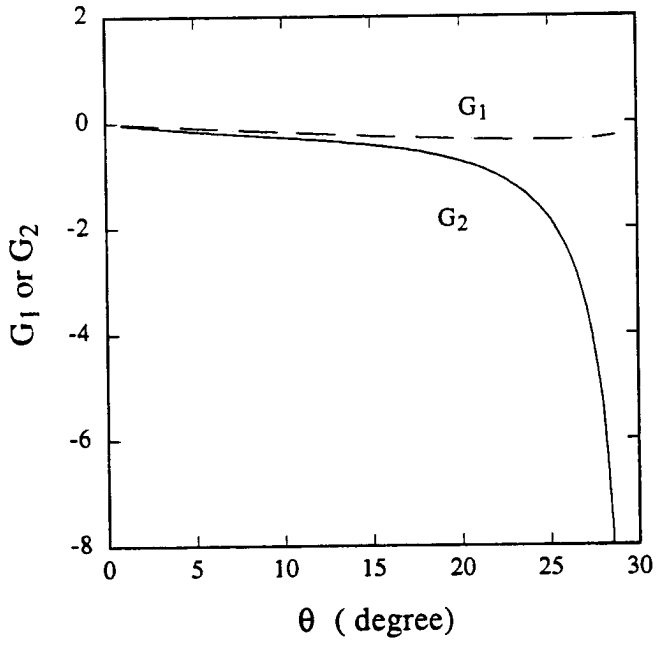


Figure 4 $G_1$ and $G_2$ versus SV-wave incident angle ($\theta$) in Bedford limestone

# 3 Experiments and Results

## 3.1 Experimental Details

The rock sample (Bedford limestone) is assembled using two blocks as shown in Figure 1. The rock sample with strain gauges is placed inside a tank pressurized to 10 bar. To prevent the sample from becoming invaded by water, a plastic film with 0.21 mm thickness (Vinyl film sheet No. 8562K5, Warp Bros.) is wrapped on the surface of the rocks. The experimental set-up is shown in Figure 5. From the recovered samples, the rocks were still dry after the explosions. The type of strain gauge used in this work is CEA-00-062UT-120 from Measurements Group. The dimensions of the gauges are 3x3 mm. The initial resistance of gauges is 120 $\Omega$ $\pm$0.4% and the gauge factor is 2.090 $\pm$ 0.5%. The procedure to attach the gauges on the surface is: (1) The surface is polished with sandpaper (No. 240, 3M); (2) the surface is cleaned using acetone; (3) the gauges are attached on the surface using 910 adhesive (Permabond International); (4) after the adhesive is dried, a thin layer of the epoxy ( 5-minute epoxy, ITWDevcon) is applied on the gauge surface in order to protect them. The voltage on the gauge is typical 6 V ( before each experiment, the voltage on each gauge is measured). The amplifiers used in this work are specially designed to satisfy the requirements of high gain, wide bandwidth and low noise.

The explosive used in this work is PETN. The explosive is placed in a plastic shell( the thickness of the shell is 1 mm, and the inner diameter is the same as the diameter of the explosives) and detonated using a high-voltage detonator ( the voltage is about 2000 V). The size of the detonator is $\phi$2x8 mm.

## 3.2 Experimental Results

Two experiments were conducted on Bedford Limestone. One modeled a decoupled explosion and the other a tamped explosion. The parameters used in the experiments are listed in Table 1.

The recorded strains for the two experiments are shown in Figures 6(a) and (b), Figures 7(a) and (b). The characteristics of the strains recorded by the gauges are the same as predicted using the

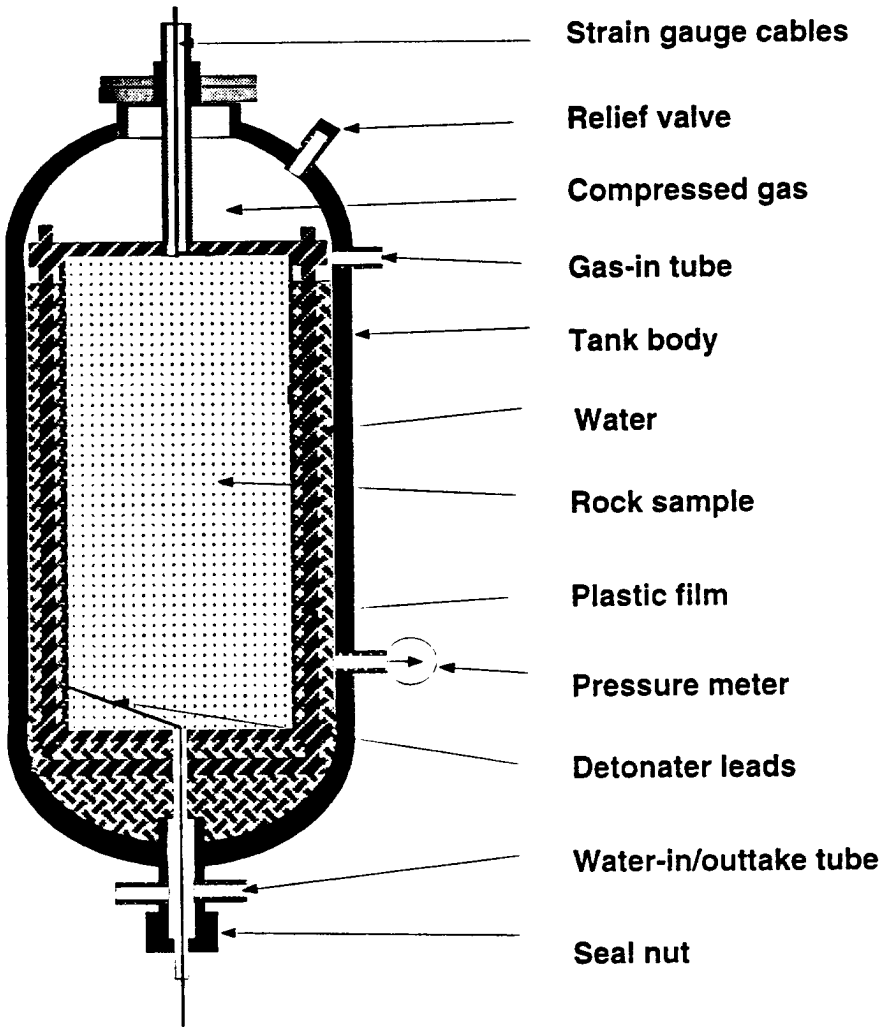


Figure 5 Pressurized test chamber

Table 1: **Parameters used in the experiments**

| | dimensions of explosives | mass of explosives | type of explosives | dimensions of cavities |
|---|---|---|---|---|
| decoupled | $\phi$ 5x6 mm | 0.24 g | pressured PETN | $\phi$ 30x30 mm |
| tamped | $\phi$10x10 mm | 1.2 g | sheet PETN | $\phi$ 12x12 mm |

Table 2: **The results for the decoupled experiment**

| $\theta^o$ | D (mm) | $\varepsilon_{sv}(\mu\varepsilon)$ | $t_{sv}(\mu s)$ | $\varepsilon_p(\mu\varepsilon)$ | $t_p(\mu s)$ | $u^I_{sv}(mm)$ | $v_{sv}(m/s)$ | $u^I_p(mm)$ | $v_p(m/s)$ | $R_u$ |
|---|---|---|---|---|---|---|---|---|---|---|
| 2.1 | 153 | | | 98 | 5 | | | 0.0072 | 1.4 | |
| 15.3 | 157 | 78 | 8 | 67 | 4 | 0.0055 | 0.7 | 0.0043 | 1.0 | 0.7 |
| 36.4 | 189 | | | 28 | | | | 0.0019 | 0.34 | |

Table 3: **The results for the tamped experiment**

| $\theta^o$ | D (mm) | $\varepsilon_{sv}(\mu\varepsilon)$ | $t_{sv}(\mu s)$ | $\varepsilon_p(\mu\varepsilon)$ | $t_p(\mu s)$ | $u^I_{sv}(mm)$ | $v_{sv}(m/s)$ | $u^I_p(mm)$ | $v_p(m/s)$ | $R_u$ |
|---|---|---|---|---|---|---|---|---|---|---|
| 6.4 | 153 | 233 | 8.8 | 450 | 16 | 0.029 | 3.3 | 0.035 | 2.2 | 1.5 |
| 9.8 | 243 | 164 | 11 | 95 | 13 | 0.027 | 2.4 | 0.0099 | 0.8 | 3 |
| 20.9 | 162 | 254 | 12 | 280 | 17 | 0.012 | 1.0 | 0.0174 | 1.0 | 1.0 |
| 36.3 | 198 | | | 140 | 12.5 | | | 0.0092 | 0.7 | |

where $D$ is the distance between the gauge and the center of the cavity, $t_{sv}$ and $t_p$ are the times at which the SV- and P-wave induced strains reach the maximum, $v_{sv}$ and $v_p$ are the average particle velocities for SV- and P- waves, $R_u$ is the ratio of SV-wave particle velocity to P-wave particle velocity.

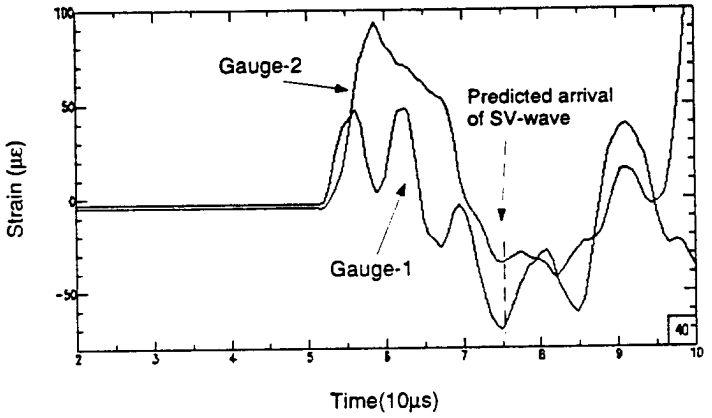


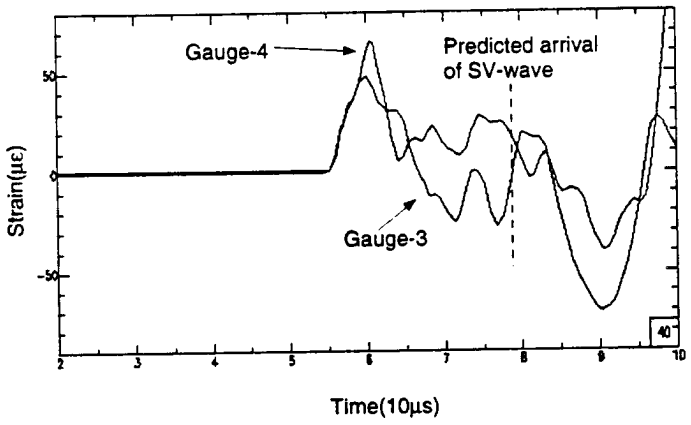


Figure 6 (a) The wave profiles from gages 1-4

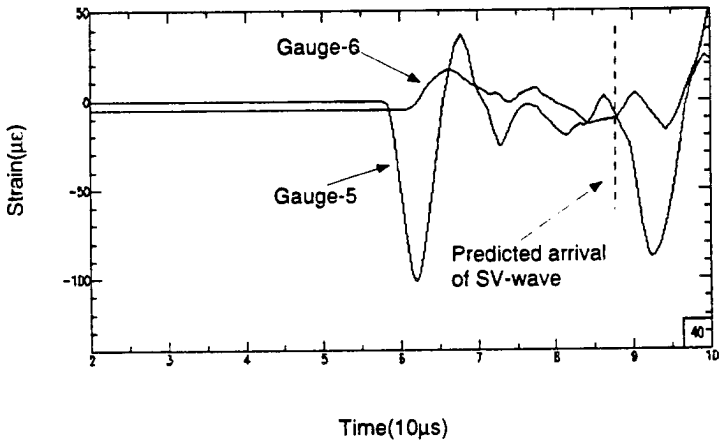


Figure 6 (b) The wave profiles from gauges 5 and 6

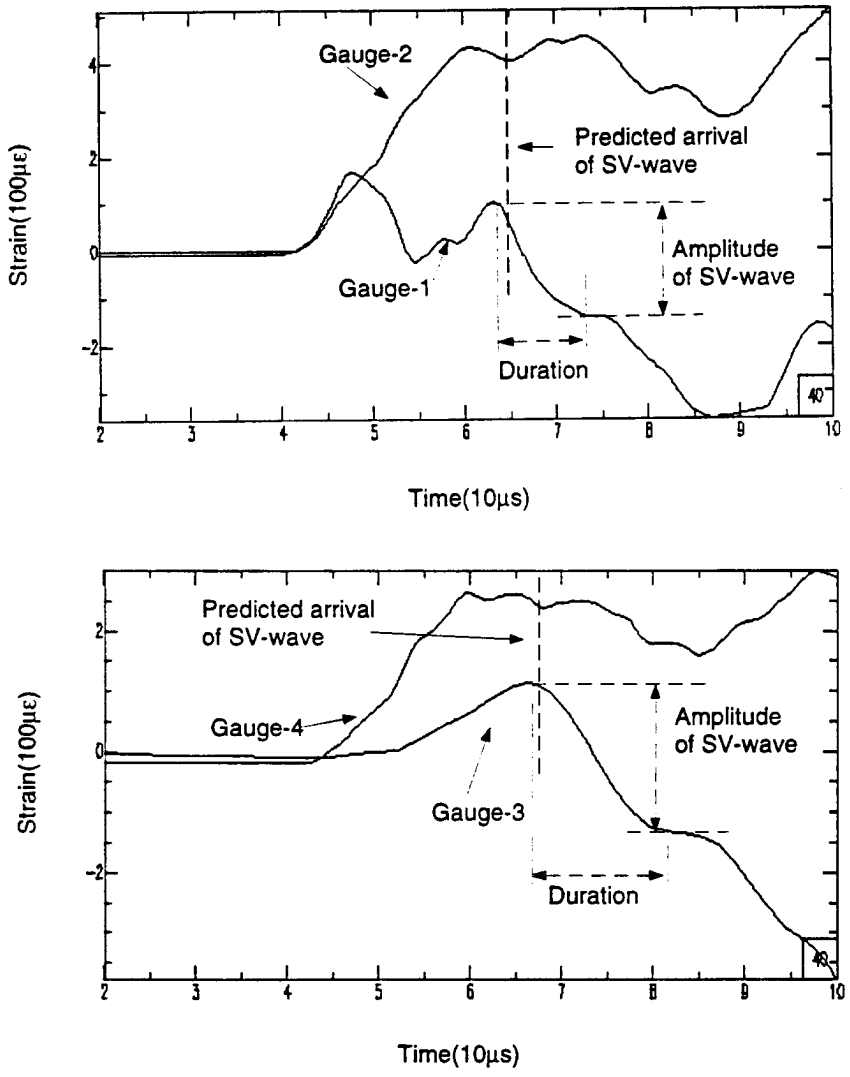


Figure 7 (a) The wave profiles from the gauge 1- 4

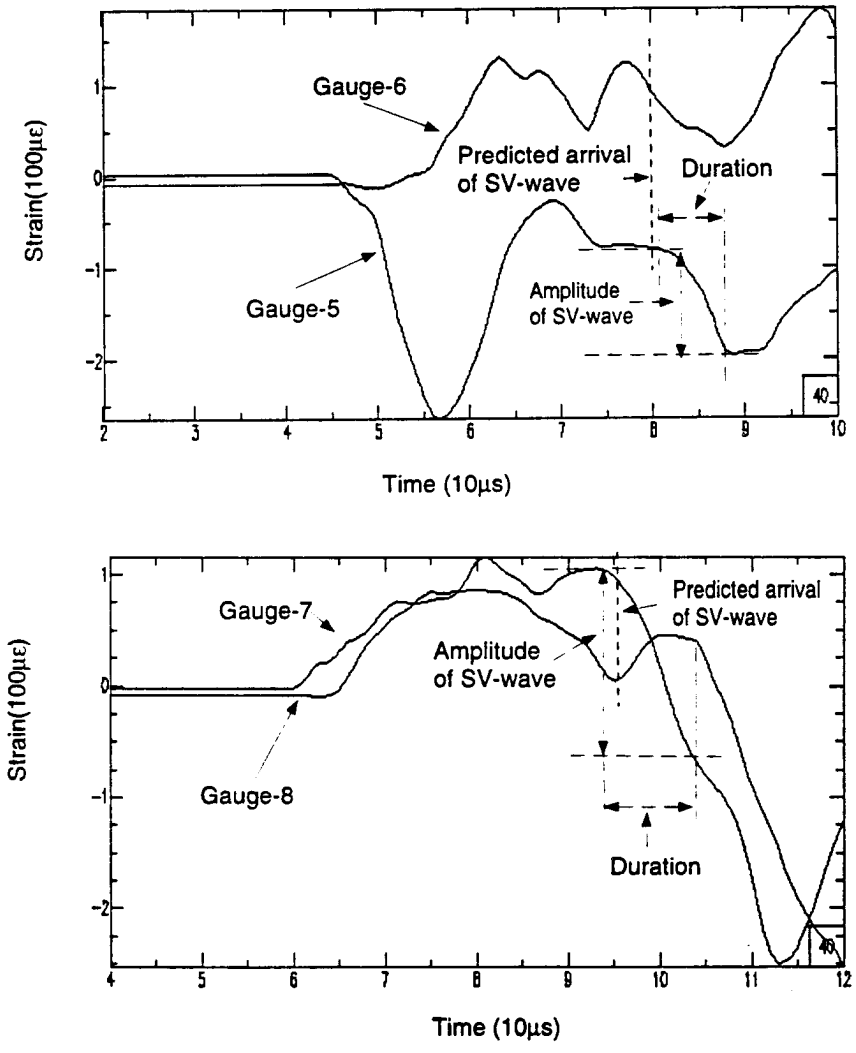


Figure 7 (b) The wave profiles from gauges 5 - 8

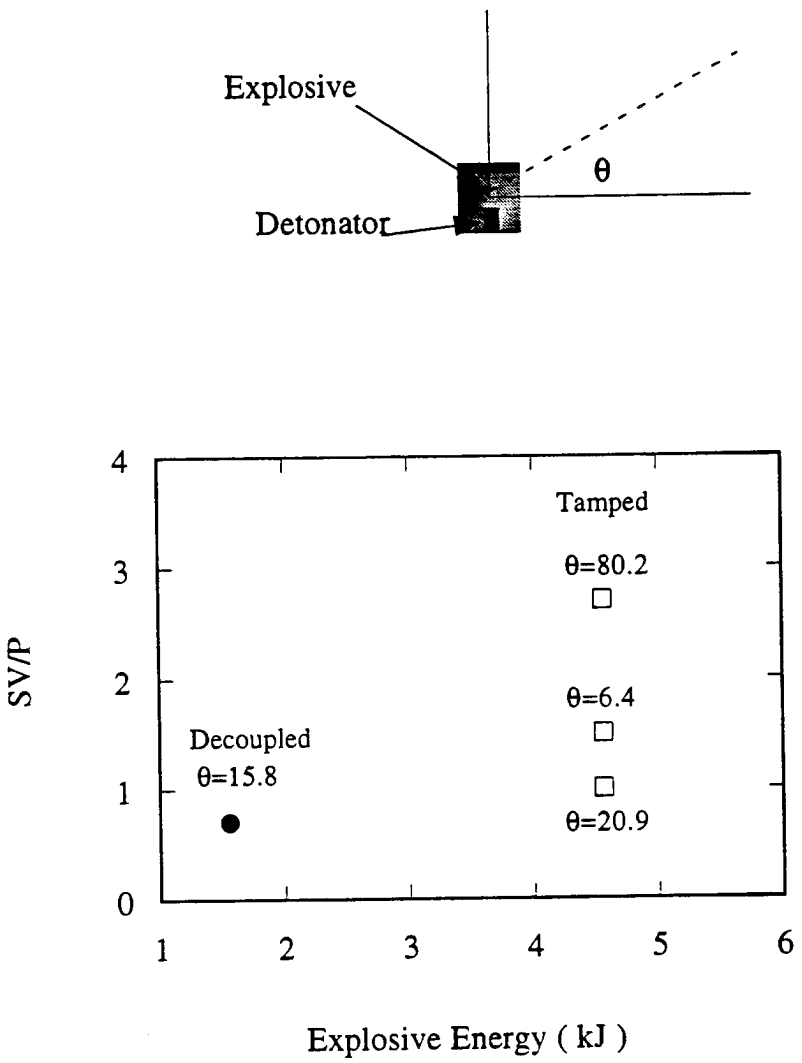


Figure 8 Ratio of SV- to P-wave particle velocity, SV/P, versus explosive energy

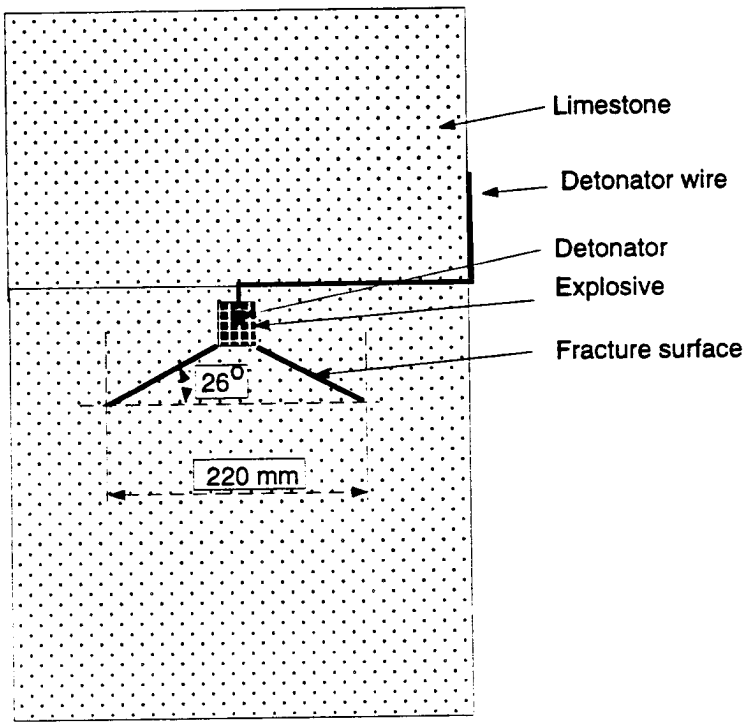


Figure 9 Profile of fracture surface from the tamped experiment.

derived expressions (Eqs. (26), (37), (39) and (41)), e.g., the strains along direction 1 induced by incident P-waves are always positive, and the strains along the direction 2 changed polarities with increasing P-wave incident angle as shown in Figures 6(b) and 7(b). The strains induced by incident SV-waves are much larger along direction 2 than direction 1 and are negative along direction 2 as shown in Figures 7(a) and (b). These experiment results verify that the method developed in this work can be used to monitor the P- and SV-waves generated from explosions in rocks.

From the records, it is straightforward to determine the SV-wave amplitude from the tamped experiment. It is difficult to get the SV-wave amplitude for the decoupled experiments, because it seems that there are several waves mixed with SV-waves. From the P- and SV-wave velocities of Bedford limestone ($\alpha = 4.9$ (km/s), $\beta = 2.8$(km/s)), the expected S-wave arrivals are labeled on the records. The time difference between the expected and the recorded is less than $2\mu s$ for the tamped experiment, but it is hard to observe SV-wave arrival around the expected time for the decoupled experiment. The relationship between the ratio of average P-wave particle velocity to SV-wave particle velocity and the energy for the two experiments is shown in Figure 8. The experiment results are listed in the Tables 2 and 3.

The recovered samples indicate minimal damage occurred in the decoupled experiment near the cavity, but symmetric explosion-induced tensional fracture occurred in the tamped experiment. The profile of the fracture is shown in Figure 9. This tensional fracture is initiated by the interaction between shock waves and the cylindrical cavity surface at the corner and is further developed by the penetration of the high pressure explosion products. From the profile of the cavity used in Sterling explosion (Langston, 1983), this tensional fracture may occur around the intersection between the inner surface of the cylindric-like cavity and the free surface of the recrystallized salt and also around the pre-existing crack zone on the top of the cavity. These fractures should generate P- and SV-waves, and these waves can explain the polarity change of SV-waves and the second P-wave that appears to be generated beneath the bottom of the cavity.

From the records, the waves generated in the decoupled experiment contain relatively higher frequencies than those in the tamped experiment. The reasons may include: (1) the width of the shock waves acting on the inner surface of the rocks for the decoupled experiment is narrower than that of the shock wave for the tamped experiment. This is due to the difference between the initial dimensions of the explosive and the ratio of the volume of the explosive to the volume of the cavity. We intend to analyze this in more detail; (2) the elastic deformation radius may be larger for the tamped explosion than it is for the decoupled explosion.

# 4 Conclusions

From the first two experiments, we conclude:

1. The method we developed in this work can be used to monitor near source P- and SV-waves generated by explosions (with a smaller charge).
2. The waves generated in the decoupled experiment contain relatively higher frequencies than these generated in the tamped experiment. The corner frequencies of the signals need to be analyzed.
3. The efficiency of SV-wave generation from the tamped explosion is higher than that of the decoupled explosion. This may be caused by the large plastic deformation near the cavity and tensional fracture in the tamped experiment.
4. The explosion-induced tensional fracture which occurred in the tamped explosion may be used to explain some of the experimental results in the Sterling explosion.

# References

[1] Aki, K. and Richards, P., *Quantitative Seismology Theory and Methods,* W. H. Freeman and Company, 151, 1980.

[2] Coursen L., A gas penetration model of fragmentation, *Fragmentation by Blasting,* edited by Fourney W., Boade R. and Costin L., Society for Experimental Mechanics, Connecticut, 1-10, 1985.

[3] Denny M. and Goodman D., A case study of the seismic source function: Salmon and Sterling reevaluated, *J. Geophys. Res.*, 95, 19,705-19,723, 1990.

[4] Denny M. and Johnson L., The explosion seismic function: models and scaling laws reviewed, *Explosion Source Phenomenology*, edited by Taylor S., Patteron H. and Richards P., American Geophysical Union, 1-24, 1991.

[5] Florence A., Miller S. and Keller C., Decoupling of underground explosions by rubble-filled cavities, *J. Geophys. Res.*, 98, 14,197-14,209, 1993.

[6] Glenn L., Energy-density effects on seismic decoupling, *J. Geophys. Res.*, 98, 1933-1942, 1993.

[7] Glenn L. and Goldstein P., Seismic decoupling with chemical and nuclear explosions in salt, *J. Geophys. Res.*, 99, 11,732 - 11,730, 1994.

[8] Glenn L. and Goldstein P., Reply, *J. Geophys. Res.,* 101, 851-854, 1996.

[9] Glenn L., Ladd A., Moran B., and Wilson K., Elastic radiation from explosively loaded ellipsoidal cavities in an unbounded medium, *Geophys. J. R. astr. Soc.,* 81, 231- 241, 1985.

[10] Kim S., Clifton R. and Kumar P., A combined normal and transverse displacement interferometer, *J. Appl. Phys.,* 48, 4132-4139, 1977.

[11] Langston C., Kinematic analysis of strong motion P and SV waves from the Sterling event, *J. Geophys. Res.,* 88, 2486-3497, 1983.

[12] Masse R., Reviews of seismic source models for underground nuclear explosions, *Bull. Seism. Soc. Am.*, 71, 1249-1268, 1981.

[13] Murphey B., Particle motions near explosions in Halite, *J. Geophys. Res.,* 66, 947-957, 1961.

[14] Murphy J. , Types of seismic events and their source descriptions, *Monitoring a Comprehensive Test Ban Treaty,* edited by Husebye and Dainty, Kluwer Academic Publishers, the Netherlands, 247-293, 1996.

[15] Murphy J., Rimer N. and Stevens J., Comment on " Seismic decoupling with chemical and nuclear explosions in salt" by L. Glenn and P. Goldstein, *J. Geophys. Res.,* 101, 845-850, 1996.

[16] Sykes L., Dealing with decoupled nuclear explosions under a comprehensive test ban treaty, *Monitoring a Comprehensive Test Ban Treaty,* edited by Husebye and Dainty, Kluwer Academic Publishers, the Netherlands, 225-245, 1996.

[17] Walter W., Mayeda K. and Patton H., Phase and spectral ratio discrimination between NTS earthquakes and explosions. Part I: empirical observation, *Bull. Seism. Soc. Am.,* 85, 1050-1067, 1995.

THOMAS AHRENS
SEISMOLOGICAL LABORATORY 252-21
CALIFORNIA INSTITUTE OF TECHNOLOGY
PASADENA, CA 91125

SHELTON ALEXANDER
PENNSYLVANIA STATE UNIVERSITY
DEPARTMENT OF GEOSCIENCES
537 DEIKE BUILDING
UNIVERSITY PARK, PA 16801

T.G. BARKER
MAXWELL TECHNOLOGIES
8888 BALBOA AVE.
SAN DIEGO, CA 92123-1506

THERON J. BENNETT
MAXWELL TECHNOLOGIES
11800 SUNRISE VALLEY DRIVE SUITE 1212
RESTON, VA 22091

JONATHAN BERGER
UNIVERSITY OF CA, SAN DIEGO
SCRIPPS INSTITUTION OF OCEANOGRAPHY IGPP, 0225
9500 GILMAN DRIVE
LA JOLLA, CA 92093-0225

STEVEN BRATT
NTPO
1901 N. MOORE STREET, SUITE 609
ARLINGTON, VA 22209

LESLIE A. CASEY
DOE
1000 INDEPENDENCE AVE. SW
NN-20
WASHINGTON, DC 20585-0420

STANLEY DICKINSON
AFOSR
110 DUNCAN AVENUE, SUITE B115
BOLLING AFB
WASHINGTON, D.C. 20332-001

RICHARD J. FANTEL
BUREAU OF MINES
DEPT OF INTERIOR, BLDG 20
DENVER FEDERAL CENTER
DENVER, CO 80225

ROBERT GEIL
DOE
PALAIS DES NATIONS, RM D615
GENEVA 10, SWITZERLAND

RALPH ALEWINE
NTPO
1901 N. MOORE STREET, SUITE 609
ARLINGTON, VA 22209

MUAWIA BARAZANGI
INSTITUTE FOR THE STUDY OF THE CONTINENTS
3126 SNEE HALL
CORNELL UNIVERSITY
ITHACA, NY 14853

DOUGLAS BAUMGARDT
ENSCO INC.
5400 PORT ROYAL ROAD
SPRINGFIELD, VA 22151

WILLIAM BENSON
NAS/COS
ROOM HA372
2001 WISCONSIN AVE. NW
WASHINGTON, DC 20007

ROBERT BLANDFORD
AFTAC
1300 N. 17TH STREET
SUITE 1450
ARLINGTON, VA 22209-2308

RHETT BUTLER
IRIS
1200 NEW YORK AVE., NW
SUITE 800
WASHINGTON, DC 20005

CATHERINE DE GROOT-HEDLIN
UNIVERSITY OF CALIFORNIA, SAN DIEGO
INSTITUTE OF GEOPHYSICS AND PLANETARY PHYSICS
8604 LA JOLLA SHORES DRIVE
SAN DIEGO, CA 92093

DIANE I. DOSER
DEPARTMENT OF GEOLOGICAL SCIENCES
THE UNIVERSITY OF TEXAS AT EL PASO
EL PASO, TX 79968

MARK D. FISK
MISSION RESEARCH CORPORATION
735 STATE STREET
P.O. DRAWER 719
SANTA BARBARA, CA 93102-0719

LORI GRANT
MULTIMAX, INC.
311C FOREST AVE. SUITE 3
PACIFIC GROVE, CA 93950

HENRY GRAY
SMU STATISTICS DEPARTMENT
P.O. BOX 750302
DALLAS, TX 75275-0302

I. N. GUPTA
MULTIMAX, INC.
1441 MCCORMICK DRIVE
LARGO, MD 20774

DAVID HARKRIDER
PHILLIPS LABORATORY
EARTH SCIENCES DIVISION
29 RANDOLPH ROAD
HANSCOM AFB, MA 01731-3010

IAN MACGREGOR
NSF
4201 WILSON BLVD., ROOM 785
ARLINGTON, VA 22230

THOMAS HEARN
NEW MEXICO STATE UNIVERSITY
DEPARTMENT OF PHYSICS
LAS CRUCES, NM 88003

MICHAEL HEDLIN
UNIVERSITY OF CALIFORNIA, SAN DIEGO
SCRIPPS INSTITUTION OF OCEANOGRAPHY IGPP, 0225
9500 GILMAN DRIVE
LA JOLLA, CA 92093-0225

DONALD HELMBERGER
CALIFORNIA INSTITUTE OF TECHNOLOGY
DIVISION OF GEOLOGICAL & PLANETARY SCIENCES
SEISMOLOGICAL LABORATORY
PASADENA, CA 91125

EUGENE HERRIN
SOUTHERN METHODIST UNIVERSITY
DEPARTMENT OF GEOLOGICAL SCIENCES
DALLAS, TX 75275-0395

ROBERT HERRMANN
ST. LOUIS UNIVERSITY
DEPARTMENT OF EARTH & ATMOSPHERIC SCIENCES
3507 LACLEDE AVENUE
ST. LOUIS, MO 63103

VINDELL HSU
HQ/AFTAC/TTR
1030 S. HIGHWAY A1A
PATRICK AFB, FL 32925-3002

ANTHONY IANNACCHIONE
BUREAU OF MINES
COCHRANE MILL ROAD
PO BOX 18070
PITTSBURGH, PA 15236-9986

RONG-SONG JIH
HQ DSWA/PMP/CTBT
6801 TELEGRAPH ROAD
ALEXANDRIA, VA 22310-3398

THOMAS JORDAN
MASSACHUSETTS INSTITUTE OF TECHNOLOGY
EARTH, ATMOSPHERIC & PLANETARY SCIENCES
77 MASSACHUSETTS AVENUE, 54-918
CAMBRIDGE, MA 02139

LAWRENCE LIVERMORE NATIONAL LABORATORY
ATTN: TECHNICAL STAFF (PLS ROUTE)
PO BOX 808, MS L-200
LIVERMORE, CA 94551

LAWRENCE LIVERMORE NATIONAL LABORATORY
ATTN: TECHNICAL STAFF (PLS ROUTE)
PO BOX 808, MS L-221
LIVERMORE, CA 94551

LAWRENCE LIVERMORE NATIONAL LABORATORY
ATTN: TECHNICAL STAFF (PLS ROUTE)
LLNL
PO BOX 808, MS L-175
LIVERMORE, CA 94551

LAWRENCE LIVERMORE NATIONAL LABORATORY
ATTN: TECHNICAL STAFF (PLS ROUTE)
PO BOX 808, MS L-208
LIVERMORE, CA 94551

LAWRENCE LIVERMORE NATIONAL LABORATORY
ATTN: TECHNICAL STAFF (PLS ROUTE)
PO BOX 808, MS L-202
LIVERMORE, CA 94551

LAWRENCE LIVERMORE NATIONAL LABORATORY
ATTN: TECHNICAL STAFF (PLS ROUTE)
PO BOX 808, MS L-195
LIVERMORE, CA 94551

LAWRENCE LIVERMORE NATIONAL LABORATORY
ATTN: TECHNICAL STAFF (PLS ROUTE)
PO BOX 808, MS L-205
LIVERMORE, CA 94551

THORNE LAY
UNIVERSITY OF CALIFORNIA, SANTA CRUZ
EARTH SCIENCES DEPARTMENT
EARTH & MARINE SCIENCE BUILDING
SANTA CRUZ, CA 95064

ATTN: LIBRARIAN
CENTER FOR MONITORING RESEARCH
1300 N. 17th STREET, SUITE 1450
ARLINGTON, VA 22209

LOS ALAMOS NATIONAL LABORATORY
ATTN: TECHNICAL STAFF (PLS ROUTE)
PO BOX 1663, MS F659
LOS ALAMOS, NM 87545

LOS ALAMOS NATIONAL LABORATORY
ATTN: TECHNICAL STAFF (PLS ROUTE)
PO BOX 1663, MS D460
LOS ALAMOS, NM 87545

GARY MCCARTOR
SOUTHERN METHODIST UNIVERSITY
DEPARTMENT OF PHYSICS
DALLAS, TX 75275-0395

BRIAN MITCHELL
DEPARTMENT OF EARTH & ATMOSPHERIC SCIENCES
ST. LOUIS UNIVERSITY
3507 LACLEDE AVENUE
ST. LOUIS, MO 63103

JOHN MURPHY
MAXWELL TECHNOLOGIES
11800 SUNRISE VALLEY DRIVE SUITE 1212
RESTON, VA 22091

JAMES NI
NEW MEXICO STATE UNIVERSITY
DEPARTMENT OF PHYSICS
LAS CRUCES, NM 88003

PACIFIC NORTHWEST NATIONAL LABORATORY
ATTN: TECHNICAL STAFF (PLS ROUTE)
PO BOX 999, MS K6-48
RICHLAND, WA 99352

PACIFIC NORTHWEST NATIONAL LABORATORY
ATTN: TECHNICAL STAFF (PLS ROUTE)
PO BOX 999, MS K6-84
RICHLAND, WA 99352

ANATOLI L. LEVSHIN
DEPARTMENT OF PHYSICS
UNIVERSITY OF COLORADO
CAMPUS BOX 390
BOULDER, CO 80309-0309

DONALD A. LINGER
DNA
6801 TELEGRAPH ROAD
ALEXANDRIA, VA 22310

LOS ALAMOS NATIONAL LABORATORY
ATTN: TECHNICAL STAFF (PLS ROUTE)
PO BOX 1663, MS F665
LOS ALAMOS, NM 87545

LOS ALAMOS NATIONAL LABORATORY
ATTN: TECHNICAL STAFF (PLS ROUTE)
PO BOX 1663, MS C335
LOS ALAMOS, NM 87545

KEITH MCLAUGHLIN
MAXWELL TECHNOLOGIES
8888 BALBOA AVE.
SAN DIEGO, CA 92123-1506

RICHARD MORROW
USACDA/IVI
320 21ST STREET, N.W.
WASHINGTON, DC 20451

ROBERT NORTH
CENTER FOR MONITORING RESEARCH
1300 N. 17th STREET, SUITE 1450
ARLINGTON, VA 22209

JOHN ORCUTT
INSTITUTE OF GEOPHYSICS AND PLANETARY PHYSICS
UNIVERSITY OF CALIFORNIA, SAN DIEGO
LA JOLLA, CA 92093

PACIFIC NORTHWEST NATIONAL LABORATORY
ATTN: TECHNICAL STAFF (PLS ROUTE)
PO BOX 999, MS K6-40
RICHLAND, WA 99352

PACIFIC NORTHWEST NATIONAL LABORATORY
ATTN: TECHNICAL STAFF (PLS ROUTE)
PO BOX 999, MS K5-12
RICHLAND, WA 99352

FRANK PILOTTE
HQ/AFTAC/TT
1030 S. HIGHWAY A1A
PATRICK AFB, FL 32925-3002

JAY PULLI
BBN
1300 NORTH 17TH STREET
ROSSLYN, VA 22209

DAVID RUSSELL
HQ AFTAC/TTR
1030 SOUTH HIGHWAY A1A
PATRICK AFB, FL 32925-3002

SANDIA NATIONAL LABORATORY
ATTN: TECHNICAL STAFF (PLS ROUTE)
DEPT. 5704
MS 0979, PO BOX 5800
ALBUQUERQUE, NM 87185-0979

SANDIA NATIONAL LABORATORY
ATTN: TECHNICAL STAFF (PLS ROUTE)
DEPT. 5704
MS 0655, PO BOX 5800
ALBUQUERQUE, NM 87185-0655

THOMAS SERENO JR.
SCIENCE APPLICATIONS INTERNATIONAL CORPORATION
10260 CAMPUS POINT DRIVE
SAN DIEGO, CA 92121

ROBERT SHUMWAY
410 MRAK HALL
DIVISION OF STATISTICS
UNIVERSITY OF CALIFORNIA
DAVIS, CA 95616-8671

DAVID SIMPSON
IRIS
1200 NEW YORK AVE., NW
SUITE 800
WASHINGTON, DC 20005

BRIAN SULLIVAN
BOSTON COLLEGE
INSITUTE FOR SPACE RESEARCH
140 COMMONWEALTH AVENUE
CHESTNUT HILL, MA 02167

NAFI TOKSOZ
EARTH RESOURCES LABORATORY, M.I.T.
42 CARLTON STREET, E34-440
CAMBRIDGE, MA 02142

KEITH PRIESTLEY
DEPARTMENT OF EARTH SCIENCES
UNIVERSITY OF CAMBRIDGE
MADINGLEY RISE, MADINGLEY ROAD
CAMBRIDGE, CB3 OEZ UK

PAUL RICHARDS
COLUMBIA UNIVERSITY
LAMONT-DOHERTY EARTH OBSERVATORY
PALISADES, NY 10964

CHANDAN SAIKIA
WOOODWARD-CLYDE FEDERAL SERVICES
566 EL DORADO ST., SUITE 100
PASADENA, CA 91101-2560

SANDIA NATIONAL LABORATORY
ATTN: TECHNICAL STAFF (PLS ROUTE)
DEPT. 9311
MS 1159, PO BOX 5800
ALBUQUERQUE, NM 87185-1159

SANDIA NATIONAL LABORATORY
ATTN: TECHNICAL STAFF (PLS ROUTE)
DEPT. 5736
MS 0655, PO BOX 5800
ALBUQUERQUE, NM 87185-0655

AVI SHAPIRA
SEISMOLOGY DIVISION
THE INSTITUTE FOR PETROLEUM RESEARCH AND GEOPHYSICS
P.O.B. 2286, NOLON 58122 ISRAEL

MATTHEW SIBOL
ENSCO, INC.
445 PINEDA COURT
MELBOURNE, FL 32940

JEFFRY STEVENS
MAXWELL TECHNOLOGIES
8888 BALBOA AVE.
SAN DIEGO, CA 92123-1506

DAVID THOMAS
ISEE
29100 AURORA ROAD
CLEVELAND, OH 44139

LAWRENCE TURNBULL
ACIS
DCI/ACIS
WASHINGTON, DC 20505

GREG VAN DER VINK
IRIS
1200 NEW YORK AVE., NW
SUITE 800
WASHINGTON, DC 20005

TERRY WALLACE
UNIVERSITY OF ARIZONA
DEPARTMENT OF GEOSCIENCES
BUILDING #77
TUCSON, AZ 85721

JAMES WHITCOMB
NSF
NSF/ISC OPERATIONS/EAR-785
4201 WILSON BLVD., ROOM785
ARLINGTON, VA 22230

JIAKANG XIE
COLUMBIA UNIVERSITY
LAMONT DOHERTY EARTH OBSERVATORY
ROUTE 9W
PALISADES, NY 10964

OFFICE OF THE SECRETARY OF DEFENSE
DDR&E
WASHINGTON, DC 20330

TACTEC
BATTELLE MEMORIAL INSTITUTE
505 KING AVENUE
COLUMBUS, OH 43201 (FINAL REPORT)

PHILLIPS LABORATORY
ATTN: RESEARCH LIBRARY/TL
5 WRIGHT STREET
HANSCOM AFB, MA 01731-3004

FRANK VERNON
UNIVERSITY OF CALIFORNIA, SAN DIEGO
SCRIPPS INSTITUTION OF OCEANOGRAPHY IGPP, 0225
9500 GILMAN DRIVE
LA JOLLA, CA 92093-0225

DANIEL WEILL
NSF
EAR-785
4201 WILSON BLVD., ROOM 785
ARLINGTON, VA 22230

RU SHAN WU
UNIVERSITY OF CALIFORNIA SANTA CRUZ
EARTH SCIENCES DEPT.
1156 HIGH STREET
SANTA CRUZ, CA 95064

JAMES E. ZOLLWEG
BOISE STATE UNIVERSITY
GEOSCIENCES DEPT.
1910 UNIVERSITY DRIVE
BOISE, ID 83725

DEFENSE TECHNICAL INFORMATION CENTER
8725 JOHN J. KINGMAN ROAD
FT BELVOIR, VA 22060-6218 (2 COPIES)

PHILLIPS LABORATORY
ATTN: GPBP
29 RANDOLPH ROAD
HANSCOM AFB, MA 01731-3010

PHILLIPS LABORATORY
ATTN: PL/SUL
3550 ABERDEEN AVE SE
KIRTLAND, NM 87117-5776 (2 COPIES)